Journal of Membrane Science & Research

journal homepage: www.msrjournal.com

Research Paper

Electric Power Generation with Reverse Electrodialysis

Yoshinobu Tanaka*

IEM Research, 1-46-3 Kamiya, Ushiku-shi, Ibaraki 300-1216, Japan

ARTICLE INFO

Received 2016-08-01
Revised 2016-10-02
Accepted 2016-10-10
Available online 2016-10-10

KEYWORDS

Ion-exchange membrane
Reverse electrodialysis
Dialysis battery
Electric power generation
Computer simulation

GRAPHICAL ABSTRACT

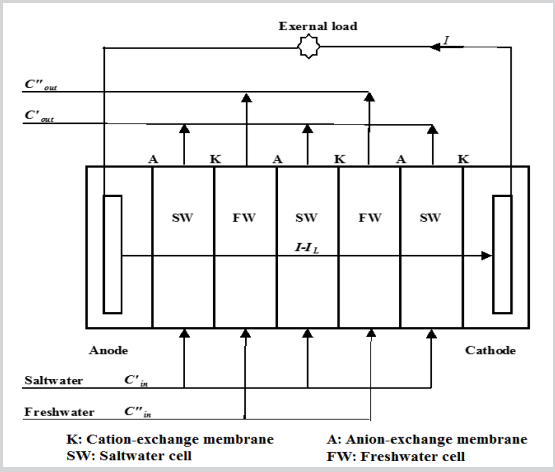

HIGHLIGHTS

- Computer program of industrial-scale RED is developed based on the ED program.
- The program is applied to RED operations supplying seawater and brackish water
- Maximum power density reaches 1.10 W/m² at 25 °C.
- Membrane pair electric resistance is less than freshwater cell resistance
- Power generation increases with electric current leakage in a RED unit.

ABSTRACT

The computer simulation program of a practical scale reverse electrodialysis process has been developed based on the program for saline water electrodialysis. The program is applied to compute the performance of an industrial-scale reverse electrodialysis stack (effective membrane area S = 1 m × 1 m = 1 m², cell pair number N = 300 pairs). The stack operating conditions are optimized. Seawater and brackish water are supplied to compute the overall membrane pair characteristics, ion and solution flux across a membrane pair, ion transport efficiency, generation efficiency, electric current leakage, stack electric resistance, stack voltage, external current, electric power, power density, pressure drop, limiting current density, and etc. When seawater (35000 ppm) and brackish water (1000 ppm) are used, the maximum power density is 0.85 W/m² (15 °C), 1.10 W/m² (25 °C) and 1.35 W/m² (35 °C). Membrane electric resistance is less than brackish water electric resistance. Electric current leakage increases the electric power generation of the RED unit. Limiting current density is very large, so the unit is operated stably. By arranging 12 stacks, a small-scale reverse electrdialysis plant (N= 12×300 = 3600 pairs) is assembled. The plant is operated to compute the performance changing external electric resistance.

1. Introduction

Reverse electrodialysis (RED) is a technology to generate electric power using salt concentration (i.e. chemical potential) difference across an ion-exchange membrane (IEM) soaked in a salt solution. It is also designated as dialysis battery and applicable at the place where concentrated and diluted solutions, such as seawater and brackish water, are supplied simultaneously. Wick and Schmit [1] estimated that the total salinity power reaches 2.6 TW, which is sufficient to supply the total electricity demand in the world (2 TW). RED is a primary battery and generates a constant direct current. Generated power is clean and sustainable. Moreover, it does not cause thermal pollution and CO_2 exhaust.

Manecke [2] started fundamental study of RED. Pattle [3] generated electric power of 0.05 W/m² from a stack integrated 47 membrane pairs. In another work, Weinstein and Leiz [4] obtained 0.33 W/m². Audinos [5] obtained 0.40 W/m². Veerman et al. [6] obtained 0.93 W/m².

* Corresponding author:
E-mail address: Fwis1202@mb.infoweb.ne.jp (Y. Tanaka)

DOI: 10.22079/jmsr.2016.22128

Clampitt and Kiviat [7], Lacy [8] and Lagur-Grodzinski and Kramer [9] developed the theory of the RED, respectively. Furthermore, Veerman et al. [10] proposed the process model to design and optimize the RED process.

Phenomena generating in RED are conceptually opposite to the electrodialysis (ED). The mechanism of RED process is considerably in common with that of the ED process. ED is the most competitive technology to desalinate brackish water of salt concentration less than about 2000 ppm to produce drinking water. It is practically applied to seawater concentration for salt manufacturing. RED can be developed based on the above ED technology. However, RED has not yet been operated in a practical-scale. The main reason to obstruct the industrialization of RED is high price of the applied membranes. This manuscript discusses the performance of practical-scale RED in order to make clear the current status of the technology based on the computer simulation program developed for saline water desalination [11]. The validity of the program has been confirmed from ED experiments and operations [12–15].

2. Principle of the RED process

2.1. Mass transport

Saltwater and freshwater are assumed to be used to a RED battery unit illustrated in Figure 1.

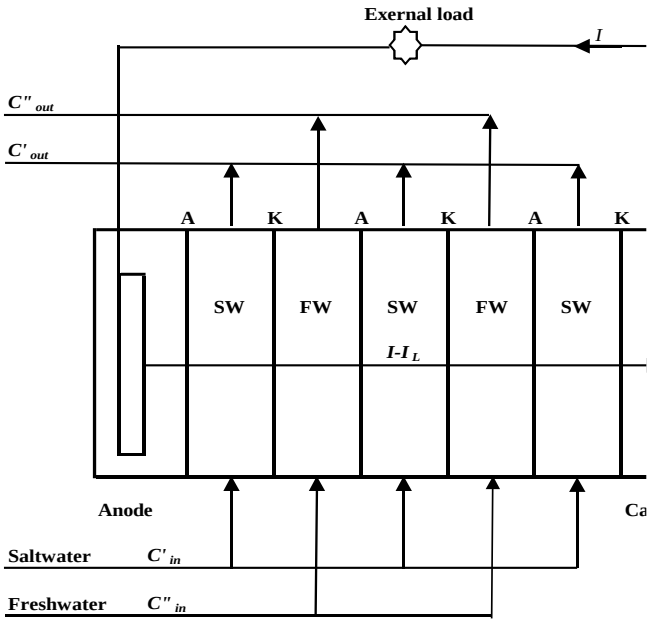

K: Cation-exchange membrane A: Anion-exchange membrane
SW: Saltwater cell FW: Freshwater cell

Fig. 1. Electric power generation with reverse electrodialysis.

The unit is incorporated with cation-exchange membranes (CEMs, K), anion-exchange membranes (AEMs, A), saltwater cells (SW cells) and freshwater cells (FW cells). SW cells and FW cells are supplied with saltwater and freshwater, respectively. I is an external electric current. Figure 2 shows the mass transport in the RED battery. $I - I_L$ is an internal electric current passing across the membranes. I_L is an electric current leakage passing through slots and ducts prepared in the cells in Figure 3.

Salt concentration is C'_{in} (C'_{out}) at the inlets (outlets) of the SW cells, and C''_{in} (C''_{out}) at the inlets (outlets) of the FW cells. Linear velocity is u'_{in} (u'_{out}) at the inlets (outlets) of SW cells and u''_{in} (u''_{out}) at the inlets (outlets) of FW cells. C' and C'' are the average salt concentration in the SW cells and the FW cells. J_S and J_V are the ion flux and solution flux passing across membrane pairs from the SW cell toward the FW cell expressed by the following overall mass transport equation [16].

$$J_S\ (\mathrm{eqcm^{-2}s^{-1}}) = \lambda i + \mu(C'-C'') = \{(t_K+t_A-1)/F\}i + \mu(C'-C'') = i/(F\eta_{memb}) \quad (1)$$

$$J_V\ (\mathrm{cms^{-1}}) = \varphi i - \rho(C'-C'') \quad (2)$$

which, i (A/cm^2) is current density. t_K and t_A are transport number of a CEM and an AEM, respectively. λ is the overall transport number, μ is the overall solute permeability, φ is the overall electro-osmotic permeability and ρ is the overall volume osmotic permeability. η_{memb} (=$i/(FJ_S)$) is the ion transport efficiency and defined as the reciprocal of the electric current efficiency η.

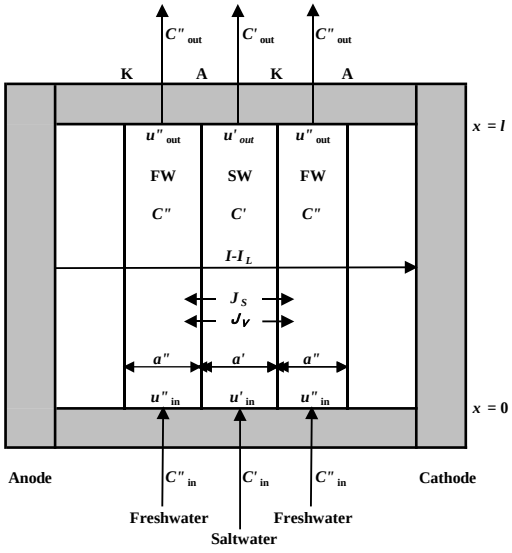

Fig. 2. Mass transport in reverse electrodialysis.

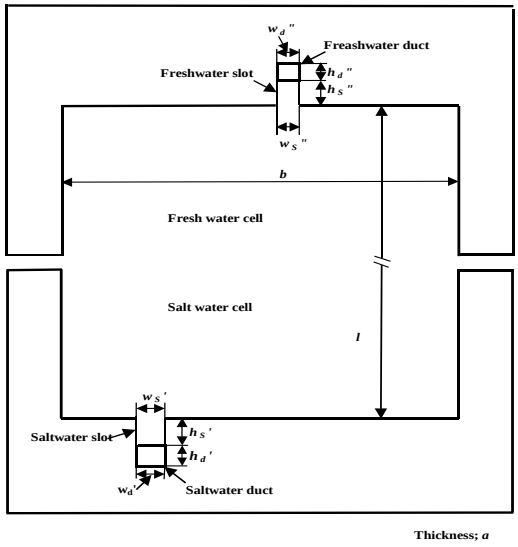

Fig. 3. Structure of a saltwater cell and a freshwater cell.

2.2. Stack electric resistance, stack voltage

A stack in RED is integrated with N cell pairs of CEMs and AEMs (SW cells and FW cells).

The stack electric resistance R_{stack} (Ω) is:

$$\frac{N}{R_{stack}} = \frac{S}{r'+r''+r_{memb}} + \frac{1}{2(r'_s+r'_d)n'} + \frac{1}{2(r''_s+r''_d)n''} \quad (3)$$

which r' and r'' (Ωcm^2) are electric resistance of a solution in the SW cell and the FW cell. r_{memb} (= r_K+r_A, Ωcm^2) is the direct current resistance of a membrane pair. n' and n'' are number of slots and ducts prepared at the head and the bottom of the SW cell and the FW cell, respectively. Moreover, r'_S and r''_S (Ωpair^{-1}) are the overall electric resistance of the SW cell slot and FW cell slot respectively.

$$\frac{1}{r'_s} = \frac{1}{r'_{s,in}} + \frac{1}{r'_{s,out}} \quad (4)$$

$$\frac{1}{r''_s} = \frac{1}{r''_{s,in}} + \frac{1}{r''_{s,out}} \quad (5)$$

In the above equations, r'_d and r''_d (Ωpair^{-1}) are the overall electric resistance of the SW cell duct and the FW cell duct, respectively.

$$\frac{1}{r'_d} = \frac{1}{r'_{d,in}} + \frac{1}{r'_{d,out}} \quad (6)$$

$$\frac{1}{r''_d} = \frac{1}{r''_{d,in}} + \frac{1}{r''_{d,out}} \quad (7)$$

Moreover, the stack voltage is:

$$V_{stack} = IR_{stack} \quad (8)$$

2.3. Circuit voltage, internal voltage, internal electric resistance

Circuit voltage V is generated in N pairs membrane cells in the RED stack. It is the driving force to generate an electric current and expresses by the following Nernst equation [17, 18].

$$V = 2\left(t_K + t_A - 1\right) N\left(\frac{RT}{F}\right)\ln\left(\frac{\gamma' C'}{\gamma'' C''}\right) \quad (9)$$

where γ' and γ'' are the salt activity in the SW cell and the FW cell, respectively.

Internal voltage V_{int} is generated in a RED battery. V_{int} is caused by electric power consumption in the battery and expressed by summing up stack voltage V_{stack} (Eq. (8)) and electrode voltage $V_{electrode}$ as follows.

$$V_{int} = V_{stack} + V_{electrode} \quad (10)$$

where $V_{electrode}$ is:

$$V_{electrode} = V_r + V_{irr} + R_\Omega I \quad (11)$$

In the above-mentioned equation, V_r ($=\Delta F/nF$) is the theoretical reversible voltage, ΔF is the free energy increase per nF Coulomb in the electrode reaction, V_{irr} is the irreversible voltage due to gas generation, concentration polarization and etc., and R_Ω is the Ohmic resistance. These parameters are sum of the values in the anode and in the cathode.

$V_{electrode}$ in Eq. (11) is the theoretical definition of the electrode voltage and it cannot be computed. However, in a practical-scale RED, membrane pair number N is increased largely and $V_{stack} >> V_{electrode}$ holds in Eq. (10). Thus, the internal electric resistance R_{int} is expressed as follows by putting $V_{int} = V_{stack}$.

$$R_{int} = V_{stack}/I \quad (12)$$

2.4. External electric current, power density, generation efficiency

Connecting the RED battery to the external load (external electric resistance) R_{ext} (Ω) forms an electric current circuit in Figure 1. The external electric current I is;

$$I(A) = \frac{V}{R_{int} + R_{ext}} \quad (13)$$

The internal electric current I^* in the RED battery is decreased from I due to the electric current leak I_L. I^* is defined by $I^* = iS$ (i is defined in Eqs. (1) and (2)) and given as follows:

$$I^* = iS = I - I_L = I\left(1 - \frac{I_L}{I}\right) \quad (14)$$

where I is the external electric current (Eq. (13)). I_L/I is the electric current leakage ratio and it is introduced by Wilson [19].

External load is electric power consumed by the external electric resistance. It corresponds to power generation W and expressed by the following equation [4]:

$$W(W) = I^2 R_{ext} = \left(\frac{V}{R_{int} + R_{ext}}\right)^2 R_{ext} \quad (15)$$

Maximum power generation W_{max} is introduced by setting $R_{ext} = R_{int}$ in Eq. (15).

$$W_{max}\,(W) = I^2 R_{int} \quad (16)$$

Power density W_d is obtained by dividing power generation W by membrane area $2SN$ (m^2) integrated into the battery.

$$W_d\left(Wm^{-2}\right) = \frac{W}{2SN} = \left(\frac{V}{R_{int} + R_{ext}}\right)^2 \left(\frac{R_{ext}}{2SN}\right) \quad (17)$$

The maximum power density $W_{d,max}$ is obtained by putting $R_{ext} = R_{int}$ in Eq. (17) [4, 8].

$$W_{d,\max}\left(Wm^{-2}\right) = \left(\frac{V^2}{4R_{int}}\right)\left(\frac{1}{2SN}\right) \quad (18)$$

Generation efficiency Eff is:

$$Eff = \frac{I^2 R_{ext}}{I^2 R_{int} + I^2 R_{ext}} = \frac{R_{ext}}{R_{int} + R_{ext}} \quad (19)$$

2.5. Ion transport efficiency

An electric current I^* (= iS) passes through the membrane with ion flux J_S. The driving force of this phenomenon is the circuit voltage V (Eq. (9)) and the ion transport efficiency through the membrane η_{memb} is defined as follows:

$$\eta_{memb} = \frac{1}{\eta} = \frac{i}{FJ_S} = \frac{I^*}{FSJ_S} \quad (20)$$

where η_{memb} is the reciprocal of the current efficiency η in ED and $\eta_{memb} > 1$ because $\eta < 1$.

The current leakage I_L is generated through slots and ducts in RED due to the circuit voltage V. I_L is ineffective in ED. However, it is effective in RED because I_L cooperates with the membrane transporting electric current I^* to generate the external electric current I ($I = I^* + I_L$). Here, the following ion transport efficiency in RED; η_{RED} is defined. η_{RED} is larger than η_{memb}; $\eta_{RED} > \eta_{memb}$.

$$\eta_{RED} = \frac{I}{FSJ_S} = \frac{I^* + I_L}{FSJ_S} \quad (21)$$

2.6. Pressure drop

Spacers mix the solution and promote the mass transfer. The specifications of the spacer are defined from a number of geometric parameters, e.g. thickness of the grid rods, the distance between the rods, and etc. Zimmerer and Kottke [20] expressed the hydraulic diameter of a spacer-filled flat channel based on the investigation in the gas flow in a wind tunnel. Based on the above investigation, the hydraulic diameter of a SW cell or FW cell, $d_{H,cell}$, and that of a SW slot or FW slot, $d_{H,slot}$, incorporated with a diagonal net spacer (see Figure 4) are expressed by the following equation.

$$d_{H,cell} = \frac{8 - \pi\frac{a}{\chi}}{4\left(\frac{1}{b} + \frac{1}{a}\right) + 2\pi\left(1 - \frac{a}{4b}\right)\frac{1}{\chi}} \quad (22)$$

$$d_{H,slot} = \frac{8 - \pi\frac{a}{\chi}}{4\left(\frac{1}{w} + \frac{1}{a}\right) + 2\pi\left(1 - \frac{a}{4w}\right)\frac{1}{\chi}} \quad (23)$$

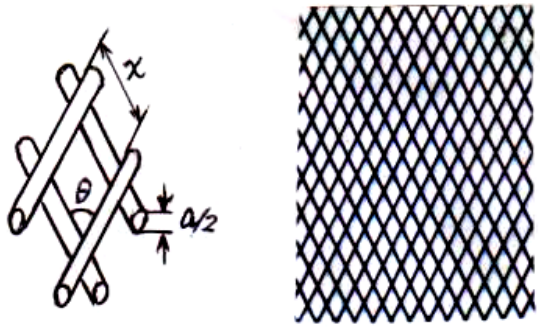

Fig. 4. Structure of a diagonal net spacer.

where *a* and *b* are the flow-pass thickness and flow-pass width in the cell and slot, respectively; *a* and *w* are the flow-pass thickness and flow-pass width in the slot, respectively. Moreover, χ is the distance between the spacer rods.

The pressure difference between the inlet and the outlet in the cell ΔP_{cell} and that in the slot ΔP_{slot} is expressed by the following equation [21]:

$$\Delta P_{cell}(Pa) = \frac{3.2\mu\, l u_{cell}}{\left(d_{H,cell}\right)^2} \tag{24}$$

$$\Delta P_{slot}(Pa) = \frac{3.2\mu\, h u_{slot}}{\left(d_{H,slot}\right)^2} \tag{25}$$

where *l* and *h* are the flow-pass length (cm) in the cell and slot, respectively. Furthermore, u_{cell} and u_{slot} are the linear velocity (cm/s) in the cell and slot, respectively. $\mu$is the viscosity coefficient of the solution (g/cm.s).

Converting the unit of the pressure difference as Pa → m;

$$\Delta H_{cell}(\mathrm{m}) = 1.01972\times10^{-4}\Delta P_{cell}(\mathrm{Pa}) \tag{26}$$

$$\Delta H_{slot}(m) = 1.01972\times10^{-4}\Delta P_{slot}(Pa) \tag{27}$$

Moreover, energy consumption is introduced as follows:

$$P_{cell}(kW) = \frac{\rho\, Q_{cell}\Delta H_{cell}}{6.12\eta_p} \tag{28}$$

$$P_{slot}(kW) = \frac{\rho\, Q_{slot}\Delta H_{slot}}{6.12\eta_p} \tag{29}$$

where ρ is the solution density. Q_{cell} and Q_{slot} are, respectively, the solution volume (m^3/min) flowing in the cell and slot. Moreover, η_p is the pump efficiency. Pump motive force *P* (= *P'* + *P''*) and pump motive force density P_d are:

$$P\ (\mathrm{kW}) = P'+P'' = (P'_{cell}+P'_{slot})+(P''_{cell}+P''_{slot}) \tag{30}$$

and

$$P_d\ (\mathrm{W/m^2}) = P/2SN \tag{31}$$

2.7. Limiting current density

Salt concentration is decreased due to concentration polarization in the boundary layer formed on the membrane surface in the SW cell. The limiting current density $(I/S)_{\mathrm{lim}}$ is expressed by the following equation [22]:

$$\left(\frac{I}{S}\right)_{\mathrm{lim}} = \left\{l_1 + l_2\left(\frac{T}{25}\right) + l_3\left(\frac{T}{25}\right)^2\right\}\frac{\left(m_1 + m_2 u'^{\#}_{out}\right)}{\zeta_{out}}\left(C'^{\#}_{out}\right)^{n_1+n_2u^{\#}_{out}} \tag{32}$$

where the superscript # denotes the least value in desalting cells in a stack.

3. Computer simulation

The principle of the RED for electric current generation is the reverse of the ED for saline water desalination or concentration. Thus, the computer program for the RED is developed on the basis of the program developed for the ED [23, 24]. In order to operate ED stably, current density *I/S* must be less than the limiting current density $(I/S)_{\mathrm{lim}}$. The $(I/S)_{\mathrm{lim}}$ item in ED is influenced by the solution velocity distribution in desalting cells. In order to compute $(I/S)_{\mathrm{lim}}$ in ED, definitely, the program of ED is developed assuming that the solution velocity ratio in desalting cells is expressed by the normal distribution. When seawater is supplied to the SW cells in RED, it is unnecessary to compute $(I/S)_{\mathrm{lim}}$, definitely, because $(I/S)_{\mathrm{lim}}$ exceeds *I/S*, largely. As a result, the solution velocity ratio in SW cells is assumed to be constant in the RED program. This assumption simplifies the program and does not influence the performance of RED, significantly.

Figure 5 shows the RED program chart and it consists of the following 15 steps. The explanation of each step should be carried out with equations. However, if many equations are included in the steps, they cause confusion. The equations are explained in the references [11], [23] and [24].

Step 1
Compute λ, μ, φ and ρ.

Step 2
Compute *C'*, *C''*, *u'* and *u''*.

Step 3
Compute C'_{out}, C''_{out}, u'_{out} and u''_{out}.

Step 4 (Decision point 1)
Control key is inputted into Point 1. If the equality is attained, the computation loops back to Point 1. If the equality is not attained, the computation proceeds to Step 5.

Step 5
Compute J_S, J_V, η_{memb}, η_{RED} and $t_K + t_A$.

Step 6
Compute *r'*, *r''* and r_{memb}.

Step 7
Compute r_s', r''_s, r'_d, r''_d and I_L/I

Step 8
Compute R_{stack} and V_{stack}.

Step 9
Compute *V*.

Step 10
Compute V_{int} and R_{int}.

Step 11
Compute *I*.

Step 12 (Decision point 2)
If the equality in Decision point 2 is not attained, the computation goes to Step 13. If the equality is attained, the computation goes to Step 14.

Step 13
Inputting Control key into Point 2, *W*, W_d, $W_{d,max}$ and *Eff* are computed, and then loops back to Point 2.

Step 14
Compute P'_{cell}, P'_{slot}, P''_{cell}, P''_{slot}, *P* and P_d.

Step 15
Compute $(I/S)_{\mathrm{lim}}$.

Computation is carried out in the spread sheet in the Appendix.
Readers can operate the program by inputting the optional input and carrying out trial-and-error calculation at the decision points (red). Computations are completed within about 10 min.

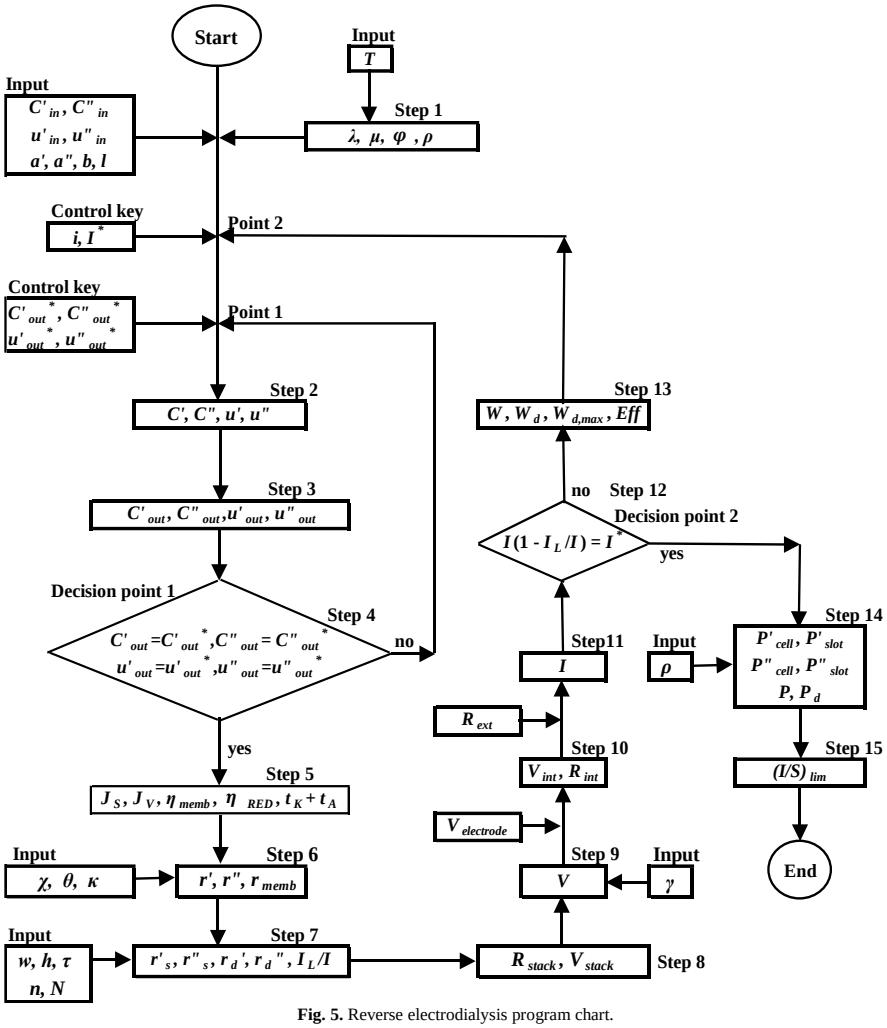

Fig. 5. Reverse electrodialysis program chart.

4. Computation

4.1. Optimization of operating conditions

Saltwater cells are supplied with seawater and freshwater cells are supplied with brackish water taken from estuary. Estuary is the sphere in which seawater and river water are contacted and mixed together. It is transition zone between the brackish water region and the seawater region. Salt concentration in the brackish water region (estuary) is 0.05–3.5% (500–35000 ppm). It is influenced by the mixing conditions of river water and seawater, and is changed with time due to tide.

Tale 1 shows the fundamental specifications and operating conditions of the RED unit. In order to decrease stack electric resistance, it is desirable to decrease the flow-pass thickness of the salt cell *a'* and of the freshwater cell *a"*. However in industrial plant manufacturing, the dimension of *a'* and *a"* has a minimum limit. Decreasing of *a'* and *a"* causes attachment of suspended materials in the feeding solution on the membrane surfaces and it increases solution flow resistance. From the standpoint of the plant manufacturing, *a'* is expected to be the same to *a"*. For operating the EDR battery stably, it is desirable to adjust u'_{in} to u''_{in} to decrease pressure difference between the salt water cells and fresh water cells.

In order to clarify the optimum *a'*, *a"*, u'_{in} and u''_{in}, the following parameters are pre-determined and $W_{d,max}$ and P_d are computed in Table 2 using the program described in Section 3 and Appendix.

a', *a"* = 0.02, 0.03, 0.04, 0.05 cm
$u'_{in} = u''_{in}$ = 2, 3, 4 cm/s
T = 25℃
C'_{in} = 35,000 ppm
C''_{in} = 1000 ppm

It is not easy to reduce the thickness of the cells in the industrial-scale unit. It is assumed that *a'*= *a"*= 0.02 cm is not applicable in the present ED technology, due to pressure drop increase with operating time. This is because suspended substances in the feeding solutions must be precipitated in the cells. The phenomena are accelerated in the unit integrated with thinner cells. The situation of RED is the same to that of ED. However, *a'*= *a"*= 0.03 cm might be possible, thus the possible cell thickness is selected as *a'*= *a"*= 0.03 cm. Actual energy density consumed in the RED process corresponds to $W_{d,max}$ – P_d and minimum energy density (i.e. optimum) conditions are achieved at *a'*= *a"*= 0.03 cm, $u'_{in} = u''_{in}$ = 3 cm/s from Table 2.

4.2. Performance of the RED stack

Seawater (C'_{in}=3500 ppm) is supplied to the salt water cells in the RED stack optimized as in section 4.1. Freshwater cells are supplied with brackish water (C''_{in} = 500, 1000, 1500, 2000 ppm) supplied from estuary. Further, we assume *a'* = *a"* = 0.03 cm, $u'_{in} = u''_{in}$ = 3 cm/s , *T* = 15 , 25, 35℃ and *N* = 300 pairs. The above parameters are inputted into the program (Section 3 and Appendix). The power generation is computed putting the external electric resistance R_{ext} = internal electric resistance R_{int}, and plotted against C''_{in} taking *T* as a parameter.

Figure 6 shows *r'*, *r"* and r_{memb}. Because of the relationship of $r'' > r_{memb} > r'$, the ratio of the membrane resistance (direct current electric resistance, r_{memb}) in the stack electric resistance R_{stack} is less than that of the freshwater cell electric resistance *r"* (see Eq. (3)). *r"* increases largely with the decrease of C''_{in}. Figure 7 shows *V*, *I* and W_{max}. *V* increases with the decrease of C''_{in} due to the Nernst equation (see Eq. (9)). In this situation, *I* decreases due to the increase of *r"* (see Figure 7). Accordingly, W_{max} does not change largely in the range of 500 < C''_{in} < 2000 ppm (see Figure 7). Figure 8 shows $W_{d,max}$ and P_d. At C''_{in} = 1000 ppm, $W_{d,max}$ becomes 0.85 W/m^2 (at 15 ℃), 1.10 W/m^2 (at 25 ℃) and 1.35 W/m^2 (at 35 ℃), respectively. P_d is, considerably, less than $W_{d,max}$. I_L/I decreases with the increase of C''_{in} (see Figure 9). Figure 10 shows η_{memb} and η_{RED}. η_{memb} decreases with C''_{in} due to the increase of *r"* (see Figure 6) caused by the decrease of I^* (Eq. (14)) in total electric current *I*. η_{RED} is larger than η_{memb} (see Figure 10); $\eta_{RED} > \eta_{memb}$.

Table 1
Fundamental specifications and operating conditions of the RED unit.

Specifications	
Flow-pass thickness of saltwater and freshwater cells a	0.05 cm
Flow-pass width of saltwater and freshwater cells b	100 cm
Flow-pass length of saltwater and freshwater cells l	100 cm
Effective membrane area $S = bl$	1 m^2
Thickness of ion-exchange membranes $\tau_K+\tau_A$	0.0450 cm
Distance between spacer rods χ	0.3 cm
Crossing angle of spacer rods θ	π /3 radian
Slot length of saltwater cells h_s'	4 cm
Slot width of saltwater cells w_s'	4 cm
Slot length of freshwater cells h_s''	4 cm
Slot width of freshwater cells w_s''	4 cm
Duct length of saltwater cells h_d'	4 cm
Duct width of saltwater cells w_d'	4 cm
Duct length of freshwater cells h_d''	4 cm
Duct width of freshwater cells w_d''	4 cm
Number of slots and ducts of saltwater cells n'	2× 8
Number of slots and ducts of freshwater cells n''	2× 8
Cell pair number N	Varied pair
Operating conditions	
Salt concentration at the inlets of saltwater cells C'_{in}	35,000 ppm
Salt concentration at the inlets of freshwater cells C''_{in}	1,000 ppm
Linear velocity at the inlets of saltwater cells u'_{in}	1 cm/s
Linear velocoty at the inlets of freshwater cells u''_{in}	1 cm/s
Temperature T	25 ℃
Pump efficiency η_p	0.7
External elecric resistance R_{ext}	Varied Ω

These phenomena are due to the electric current leakage in the RED unit and are caused by that electric resistance of the solution in slot. Moreover, the duct flow-passes in the seawater cell is less than the electric resistance of the membrane cell pairs ($r' + r'' + r_{memb}$) in the electric current passing portion. It should be strengthen that η_{RED} thus I (in Eq. (21)) and W (Eq. (15)) are increased with electric current leakage I_L. The proposed suggestions are new findings in this work.

Figure 11 shows J_S and J_V. Minus sign is supplied to J_V because J_V is transported from the freshwater cell to the saltwater cell. In J_S (see Eq. (1)), the migration term λi is predominant compared to the diffusion term $\mu(C' - C'')$. Thus J_S is decreased with C''_{in} due to the decrease of an electric current I^* (I in Figure 7). In J_V (see Eq. (2)), the electro-osmotic term φi is comparable to the volume osmosis term $\rho(C' - C'')$. Thus $-J_V$ is decreased with C''_{in} due to the decrease of I^*. However, $-J_V$ is increased with the decrease of C''_{in} due to the decrease of the volume osmosis. However, the reason of the extream appeared in Figure 11 is not understandable

4.3. RED plant operation

In Section 4.2, RED stack performance is computed setting $R_{ext} = R_{int,}$ and the power density W_d is equal to the maximum power density $W_{d,max}$. In the actual plant operation, R_{ext} is changed with time and not adjusted to R_{int}, thus the RED plant is operated at $W_d < W_{d,max}$.

In this section the following operating conditions are assumed on the basis of the computation in Section 4.2.

$a' = a'' = 0.03$ cm
$u'_{in} = u''_{in} = 3$ cm/s
$C'_{in} = 35000$ ppm
$C''_{in} = 1000$ ppm
$T = 25$ ℃

A small-scale RED plant is assembled by arranging 12 units of the stack shown in Table 1. Electric power is generated by changing R_{ext} incrementally between 2 – 40 Ω。 The results are shown in Table 3.

The maximum W and W_d are; W_{max} = 7.9 kW and $W_{d,max}$ = 1.10 W/m^2. When the external electric resistance is decreased to R_{ext} = 2 Ω, they are decreased to W = 6.2 kW and W_d = 0.86 W/m^2. When R_{ext} is increased to R_{ext} = 40 Ω, they are decreased to W = 4.2 kW and W_d = 0.59 W/m^2. It is worth quoting that the pump motive force is low.

Table 2
Optimum operating conditions.

$a' = a''$ cm	$u'_{in} = u''_{in}$ cm/s	$W_{d,max}$ W/m^2	P_d W/m^2	W_d-P_d W/m^2
0.02	2	1.0163	0.0326	0.9837
0.03		1.0388	0.0224	1.0164
0.04		0.9211	0.0173	0.9038
0.05		0.7835	0.0143	0.7692
0.02	3	1.1941	0.0732	1.1209
0.03		1.1007	0.0504	1.0503
0.04		0.9232	0.0390	0.8842
0.05		0.7684	0.0321	0.7363
0.02	4	1.2917	0.1302	1.1615
0.03		1.1177	0.0896	1.0281
0.04		0.9136	0.0693	0.8443
0.05		0.7575	0.0571	0.7004

By increasing R_{ext} from 2 Ω to 40 Ω, V is increased from 391 to 488 V and I is decreased from 56 to 10 A. J_S is decreased from 4.8×10^{-8} to 1.0×10^{-8} eq/cm^2s, $-J_V$ is increased from 0.78×10^{-6} to 5.52×10^{-6} cm/s. I_L/I is increased from 0.11 to 0.16. Moreover, η_{memb} is decreased from 1.07 to 0.94. On the other hand, η_{RED} is decreased from 1.21 to 1.12. *Eff* is increased from 0.235, via 0.500 at R_{ext} = 5.66 Ω, to 0.843. r' is increased from 0.577 to 0.699 Ωcm^2. Therefore, r'' is increased from 7.10 to 13.70 Ωcm^2, and r_{memb} is increased from 6.26 to 6.50 Ωcm^2. The relationship $r'' > r_{memb} > r'$ is still existed. C'_{out}/C'_{in} is increased from 0.91 to 0.98. C''_{out}/C''_{in} is decreased from 4.07 to 1.62. $(I/S)_{lim}$ is extremely higher than I/S. It is worth quoting that the obtained results suggest that the RED unit is operated stably without concentration polarization when sufficiently filtered seawater is supplied to SW cells. Brackish water should also be sand filtered, sufficiently, for a stable

operation.

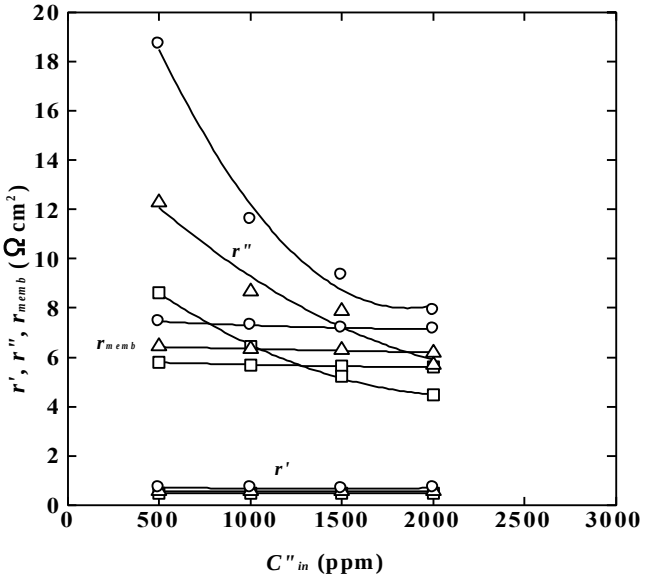

Fig. 6. r', r" and r_{memb}; T= 15 (○), 25 (△), (□) ℃.

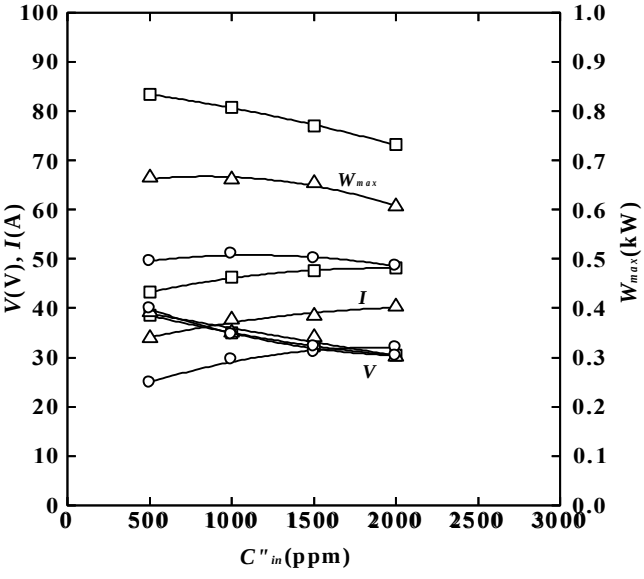

Fig. 7. *V*, *I* and W_{max}; *T* = 15 (○), 25 (△), (□) ℃

5. Conclusion

Phenomena generating in RED are conceptually opposite to ED while the mechanism of RED is considerably in common with ED. The computer simulation program of a practical-scale RED process (RED program) is developed based on the program for saline water ED (ED program). The program is applied to compute the performance of an industrial-scale RED unit. When seawater (35000 ppm) and brackish water (1000 ppm) are used in the RED, stack maximum power density is computed as 0.85 W/m^2 (15 ℃), 1.10 W/m^2 (25 ℃) and 1.35 W/m^2 (35 ℃). Limiting current density is very high, so the stack is operated stably. Electric current leakage increases the electric power generation of the RED unit. Membrane electric resistance r_{memb} is less than freshwater cell electric resistance *r''*. Thus it can be concluded that the membrane electric resistance is not controlling factor to operate the practical RED process. In order to establish the practically available RED process, it is necessary to reduce the manufacturing cost of ion-exchange membranes.

6. Nomenclatures

a	flow-pass thickness in a SW and a FW cell (cm)
b	flow-pass width in a SW and a FW cell (cm)
C	electrolyte concentraion (equiv. cm^{-3}, ppm)
d_H	hydrodynamic diameter (cm)
Eff	generation efficiency
F	Faraday constant (As equiv^{-1})
h	flow-pass length in a slot and a duct (cm)
i	current density (Acm^{-2})
I	electric current (A)
I^*	internal electric current (A)
I_L	electric current leakage (A)
I/S	average current density (Acm^{-2}, Adm^{-2})
$(I/S)_{lim}$	limiting current density (Acm^{-2}, Adm^{-2})
Js	ion flux across a membrane pair (equiv cm^{-2} s^{-1})
J_v	solution flux across a membrane pair (cm s^{-1})
l	flow-pass length in a SW and a FW cell (cm)
n	number of slot and duct in a cell
N	number of desalting cells in a stack
P	pump motive force (kW)
P_d	pump motive force density (Wm^{-2})
Q	solution flow rate (m^3 min^{-1})
r	electric resistance (Ω, Ωcm^2, Ωpair^{-1})
R	electric resistance (Ω); gas constant (JK^{-1}mol^{-1})
S	membrane area (cm^2, m^2)
t	transport number
T	temperature (℃)
u	linear velocity (cm s^{-1})
V	voltage (Volt)
w	flow-pass width in a slot and a duct (cm)
W	electric power (W)
W_d	power density (Wm^{-2})

Greek letter

γ	activity coefficient of electrolytes in a solution
ΔH	pressure difference (m)
ΔP	pressure drop (Pa)
η	current efficiency
η_{memb}	ion transport efficiency in a membrane pair
η_p	pump efficiency
η_{RED}	ion transport efficiency in RED
λ	overall transport number of a membrane pair (equiv A^{-1} s^{-1})
μ	overall solute permeability of a membrane pair (cm s^{-1})
ρ	overall volume osmotic permeability of a membrane pair (cm^{4}eq^{-1}s^{-1}); solution density (gcm^{-3})
τ	membrane thickness (cm)
φ	overall electro-osmotic permeability of a membrane pair (cm^{3}A^{-1}s^{-1})
χ	distance between spacer rods (cm)

Subscripts

A	anion-exchange membrane
cell	SW cell and FW cell
d	duct
ext	external
in	inlet
int	internal
K	cation-exchange membrane
memb	membrane pair
out	outlet
s	slot
stack	stack

Super scripts

‘	saltwater (SW) cell
“	freshwater (FW) cell
*	control key
#	the least value

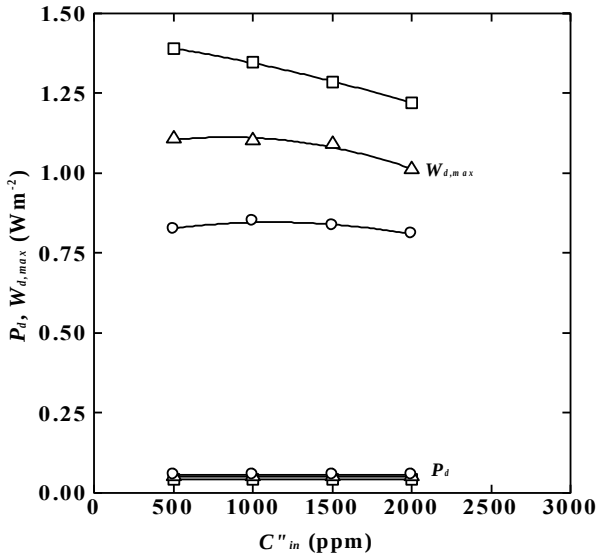

Fig. 8. $W_{d,max}$ and P_d; T= 15 (○), 25 (△), (□) ℃.

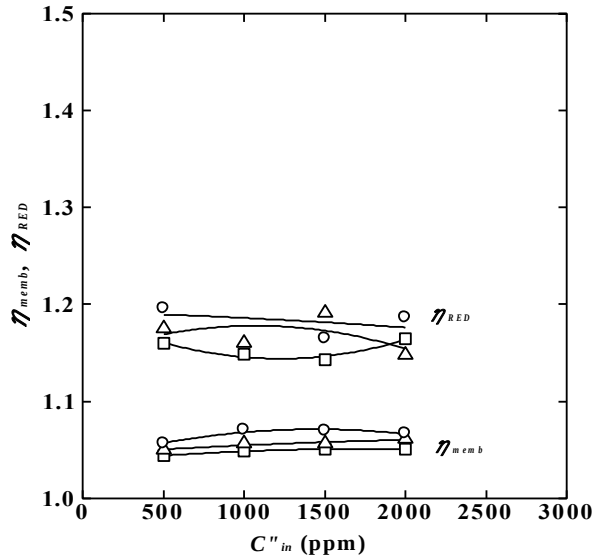

Fig. 10. η_{memb} and η_{RED}; T = 15 (○), 25 (△), (□) ℃.

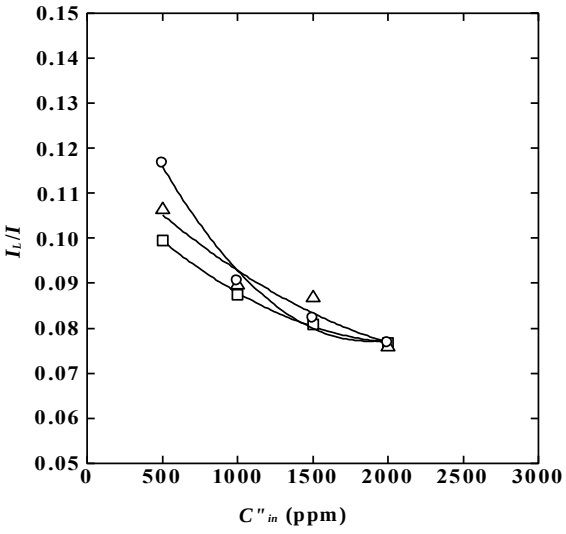

Fig. 9. I_L/I; T = 15 (○), 25 (△), (□) ℃.

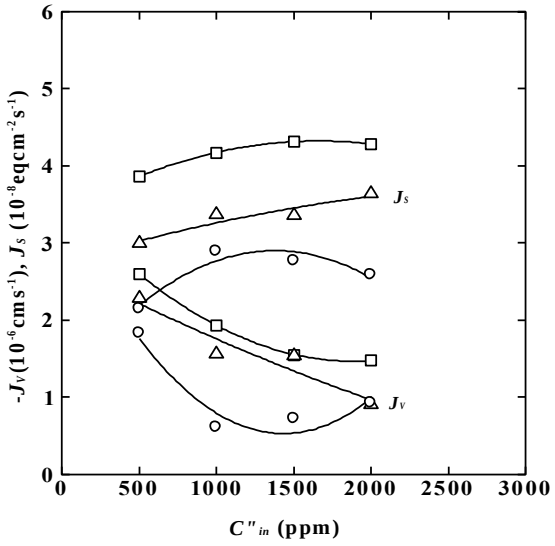

Fig. 11. J_S and J_V; T = 15 (○), 25 (△), (□) ℃.

Table 3
Relationship between external electric resistance and RED power generation (N= 12×300= 3600 pairs).

R_{ext}	Ω	2	4	5.66	8	10	20	30	40
R_{int}	Ω	5.0175	5.4055	5.6601	5.9507	6.1540	6.8242	7.2072	7.4584
W	W	6216.5	7678.1	7947.9	7843.2	7588.1	6109.3	5007.8	4228.8
W_d	W/m^2	0.8634	1.0664	1.1039	1.0893	1.0539	0.8485	0.6955	0.5873
P	W	362.7	362.8	362.8	362.8	362.8	362.8	362.8	362.8
P_d	W/m^2	0.0504	0.0504	0.0504	0.0504	0.0504	0.0504	0.0504	0.0504
$W_d - P_d$	W/m^2	0.8130	1.0160	1.0535	1.0390	1.0035	0.7981	0.6451	0.5369
V	V	391.24	412.08	424.20	436.82	444.99	468.82	480.72	487.97
I	A	55.75	43.81	37.47	31.31	27.55	17.48	12.92	10.28
J_S	10^{-8}eq/cm^{2}s	4.786	3.762	3.221	2.699	2.382	1.543	1.169	0.955
J_V	10^{-6}cm/s	-0.779	-0.904	-1.792	-2.650	-3.171	-4.550	-5.165	-5.517
I_L/I		0.1139	0.1209	0.1254	0.1305	0.1340	0.1452	0.1514	0.1554
η_{memb}		1.070	1.061	1.054	1.045	1.038	1.003	0.972	0.943
η_{RED}		1.207	1.207	1.206	1.202	1.198	1.174	1.145	1.116
Eff		0.2850	0.4253	0.5000	0.5734	0.6190	0.7456	0.8063	0.8428
r'		0.577	0.572	0.570	0.567	0.566	0.562	0.669	0.699
r''		7.103	8.144	8.829	9.613	10.162	11.976	13.016	13.699
r_{memb}		6.257	6.299	6.323	6.350	6.367	6.417	6.443	6.459
C'_{out}/C'_{in}		0.9129	0.9300	0.9390	0.9476	0.9529	0.9668	0.9729	0.9765
C''_{out}/C''_{in}		4.074	3.422	3.077	2.744	2.541	2.002	1.762	1.624
I/S	A/dm^2	0.4940	0.3852	0.3277	0.2723	0.2386	0.1494	0.1096	0.0868
$(I/S)_{lim}$	A/dm^2	35.55	36.11	36.40	36.68	36.85	37.30	37.50	37.62

7. References

[1] G. L. Wick, W. R. Schmitt, Prospects for renewable energy from sea, Mar. Technol. Soc. J. 11 (1977) 16-21.
[2] G. Manecke, Membranakkumulator, Z. Physik. Chem. 201 (1952) 1-15.
[3] R. E. Pattel, Electricity from fresh and salt water – without fuel, Chem. Proc. Eng. 35 (1955) 351-354.
[4] J. N. Weinstein, F. B. Leitz, Electric power from differences in salinity: The dialytic battery, Science 191 (1976) 557-559.
[5] R. Audinos, Inverse electrodialysis, Study of electric energy obtained starting two solutions of different salinity, J. Power Sources 10 (1983) 203-217.
[6] J. Veerman, M. Saakes, S. J. Metz, G. J. Harmsen, Reverse electrodialysis: A validated process model for design and optimization, Chem. Eng. J. 166 (2011) 256-268.
[7] B. H. Clampitt, F. E. Kiviat, Energy recovery from saline water by means of electrochemical cells, Science 194 (1976) 719-720.
[8] R. E. Lacy, Energy by reverse electrodialysis, Ocean Eng. 7 (1980) 1-47.
[9] J. Jagur-Grodzinski, R. Kramer, Novel process for direct conversion of free energy of mixing into electric power, Ind. Eng. Chem. Process Des. Dev. 25 (1986) 443-449.
[10] J. Veerman, M. Saakes, S. J. Metz, G. J. Harmsen, Reverse electrodialysis: Performance of a stack with 50 cells on the mixing of sea and river water, J. Membr. Sci. 327 (2009) 136-144.
[11] Y. Yanaka, Ion-exchange membrane electrodialysis program and its application to multi-stage continuous saline water desalination, Desalination 301 (2012) 10-25.
[12] Y. Tanaka, A computer simulation of ion exchange membranes for concentration of Seawater, Membr. Water Treat. 1 (2010) 13-37.
[13] Y. Tanaka, Ion-exchange membrane electrodialysis of saline water and its numerical Analysis, Ind. Eng. Chem. Res. 50 (2010) 10765-10777.
[14] Y. Tanaka, M. Reig,, S. Casas, C. Aladjem,, J. L. Cortina, Computer simulation of ion-exchange membrane electrodialysis for salt concentration and reduction of RO discharged brine for salt production and marine environment conservation, Desalination 367(2015) 76-89.
[15] Y. Tanaka, H. Uchino, S. Matsuda, Y. Sato, Batch ion-exchange membrane electrodialysis of mother liquid discharged from a salt-manufacturing process, Experiment and Simulation, Sep. Purif. Technol. 156 (2015) 276-287.
[16] Y. Tanaka, Irreversible thermodynamics and overall mass transport in ion-exchange membrane electrodialysis, J. Membr. Sci. 281 (2006) 517-531.
[17] W. Nernst, Zur Kinetik der losung befindlichen korper, Z. Phys. Chem. 2 (1888) 613-637.
[18] W. Nernst, Die elektromotorische wirksamkeit der ionen, Z. Phys. Chem. 4 (1889) 129-181.
[19] J. R. Wilson, Demineralization by electrodialysis, Buther-worths Scientific Publication, London, 1960, pp. 265-274.
[20] C. C. Zimmerer, V. Kottke, Effects of spacer geometry on pressure drop, mass transfer, mixing behavior, and residence time distribution, Desalination 104 (1996) 129-134.
[21] P. Tsiakis, L. G. Papageorgiou, Optimal design of an electrodialysis brackish water desalination plant, Desalination 173 (2005) 173-186.
[22] Y. Tanaka, Development of a computer simulation of batch ion-exchange membrane electrodialysis for saline water desalination, Desalination 320 (2013) 118-133.
[23] Y. Tanaka, Ion exchange membranes: Fundamentals and applications, 2nd ed., Elsevier, Amsterdam, 2015, pp. 295-322.
[24] Y. Tanaka, Saline water desalination with single-pass ion-exchange membrane electrodialysis – Computer simulation, Int. J. Comput. Softw. Eng. 1 (2016) 101, doi.org.15344/ijcse/2016/101.